Fusion Engineering and Design 124 (2017) 1118–1121

Contents lists available at ScienceDirect

Fusion Engineering and Design

journal homepage: www.elsevier.com/locate/fusengdes

Self-passivating W-Cr-Y alloys: Characterization and testing

Aida Calvo[a,*], Carmen García-Rosales[a], Nerea Ordás[a], Iñigo Iturriza[a], Karsten Schlueter[b], Freimut Koch[b], Gerald Pintsuk[c], Elena Tejado[d], José Ygnacio Pastor[d]

[a] Ceit-IK4 and TECNUN (University of Navarra), E-20018 San Sebastián, Spain
[b] Max-Planck-Institut für Plasmaphysik, D-85748 Garching, Germany
[c] Forschungszentrum Jülich GmbH, D-52425 Jülich, Germany
[d] Polytechnic University of Madrid, E-28040 Madrid, Spain

HIGHLIGHTS

- Fully dense nanocrystalline W-10Cr-0.5Y alloy produced by MA and HIP.
- Y-rich nanoparticles at GB inhibit grain growth and improve strength and toughness.
- W-10Cr-0.5Y exhibits excellent oxidation resistance under accident-like conditions.
- W-10Cr-0.5Y withstood 1000 pulses of 1 ms and 0.19 GW/m^2 at 400 °C without damage.
- 1000 pulses of 0.38 GW/m^2 result in better performance than W reference material.

ARTICLE INFO

Article history:
Received 3 October 2016
Received in revised form 31 January 2017
Accepted 1 March 2017
Available online 21 March 2017

Keywords:
Tungsten
Self-passivating alloy
Oxidation behavior
Yttrium
Thermo-shock

ABSTRACT

The use of self-passivating tungsten alloys for the first wall armor of future fusion reactors is advantageous concerning safety issues in comparison with pure tungsten. Bulk W-10Cr-0.5Y alloy manufactured by mechanical alloying followed by HIP resulted in a fully dense material with grain size around 100 nm and a dispersion of Y-rich oxide nanoparticles located at the grain boundaries. An improvement in flexural strength and fracture toughness was observed with respect to previous works. Oxidation tests under isothermal and accident-like conditions revealed a very promising oxidation behavior for the W-10Cr-0.5Y alloy. Thermo-shock tests at JUDITH-1 to simulate ELM-like loads resulted in a crack network at the surface with roughness values lower than those of a pure W reference material. An additional thermal treatment at 1550 °C improves slightly the oxidation and significantly thermo-shock resistance of the alloy.

1. Introduction

In future fusion reactors such as DEMO, a potential loss-of-coolant (LOCA) accident with simultaneous air ingress into the vacuum vessel would involve temperatures of the components above 1000 °C because of the decay heat [1]. Pure tungsten is the main candidate for the first wall armor [2]. However, under accident conditions the use of pure tungsten would lead to the formation of activated and volatile tungsten oxides, representing an important safety risk [3]. It has been demonstrated that the addition of oxide forming alloying elements to pure tungsten results in the growth of a stable protective oxide scale that prevents tungsten from oxidation at high temperatures in presence of oxygen [4–6]. Under normal operation the surface of these self-passivating alloys will consist of pure tungsten due to preferential sputtering of the alloying elements.

A recent work [7] based on previous results [6] demonstrates that a tungsten alloy of composition W-12Cr-0.5Y leads to a significant reduction of oxidation rate at temperatures ≤1000 °C, compared to those of the binary W-Cr and previously studied ternary systems. Furthermore, the dispersion of Y-rich nanoparticles observed at grain boundaries (GB) of the W matrix, refines the grain size distribution and is expected to improve the mechanical properties as reported in different works [8,9]. Furthermore, it has been shown that a Cr concentration between 8 and 13.5 wt.% in binary W–Cr alloys reduces the oxidation rate [10]. The beneficial effect of the Y_2O_3 addition on the oxidation behavior of W-Cr alloys has been also recently reported in [11].

* Corresponding author.
E-mail addresses: acalvo@ceit.es, aida.calvo.alonso@gmail.com (A. Calvo).

http://dx.doi.org/10.1016/j.fusengdes.2017.03.001

In this work, a new alloy of composition W-10Cr-0.5Y is manufactured by mechanical alloying (MA) and densified by Hot Isostatic Pressing (HIP). The alloy is subjected to a subsequent thermal treatment (TT) to dissolve the Cr-rich phase and achieve a single bcc phase [7], in agreement with the W-Cr phase diagram [12]. Microstructural investigations and microhardness of the alloy after HIP and after the TT are presented and compared to the W-12Cr-0.5Y alloy. Thermal conductivity and flexural strength of as-HIPped material are also shown. Results of oxidation tests at various conditions and thermo-shock tests at JUDITH-1 (Juelich Divertor Test Facility Hot Cells) [13] are included.

2. Experimental details

Elemental powders of pure W (99.95%, 15–30 μm), Cr (99.95%, 74 μm) and Y (99.9%, 20–30 μm) were used to produce samples of composition W-10Cr-0.5Y in wt.%. The starting powders were mechanically alloyed under Ar in a planetary ball mill using WC grinding jars and balls. The MA parameters were those found as optimum for the W-Cr-Y system in [7]. Metallic capsules with the alloyed powder were evacuated, degassed, sealed and HIPed at 1250 °C for 2 h at 150 MPa. A thermal treatment on HIPed samples was performed at 1550 °C under H_2 for 2 h. The oxygen and nitrogen contents of powders and bulk materials were determined using the inert gas fusion method (ASTM E1569), and the carbon content by the combustion method (ASTM E1019). Powders and bulk samples were characterized by field emission gun (FEG)-SEM and energy dispersive X-ray spectroscopy (EDS). The relative density of the samples was determined from the geometrical and theoretical densities, the latter obtained by the inverse rule of mixtures. The average grain size of dense materials was determined by quantitative metallography. Vickers microhardness was measured applying a load of 0.5 kg for 5 s. Three-point bending tests (3PBT) were performed on smooth and single edge laser-notched beams [14] (nominal dimensions $1.8 \times 1.8 \times 20\,mm^3$) over the temperature range 20 °C to 1100 °C under high vacuum. All tests were performed in displacement control at a fixed loading rate of 100 μm/min with 16 mm span width. Flexural strength was computed by Euler–Bernoulli equations for slender beams up to failure. To calculate the fracture toughness (KIC), the maximum load and the initial notch length for each test, measured previously via FEG-SEM, were computed in the formula proposed by Guinea et al. [15]. The thermal conductivity was obtained by the laser flash method. Isothermal oxidation tests at 800 °C and 1000 °C for up to 60 h were performed by thermogravimetric analysis (TGA). Tests under accident-like conditions, described in [7], were also done. Surfaces and cross sections of the oxidized samples were analyzed by FEG-SEM and Focused Ion Beam (FIB). Thermo-shock tests were performed at the electron beam facility JUDITH-1 [13] on samples of dimensions $10 \times 10 \times 4\,mm^3$, which were exposed at a base temperature of 400 °C to ELM-like loads consisting of 1000 pulses with power densities of 0.19 and 0.38 GW/m^2 for 1 ms, and to a disruption-like load of 1.13 GW/m^2 for 5 ms. To ensure a homogeneous loading, a small area ($4 \times 4\,mm^2$) was scanned with a focused electron beam at very high scanning frequencies. After exposure, the surface and cross section of the samples were investigated by optical microscopy.

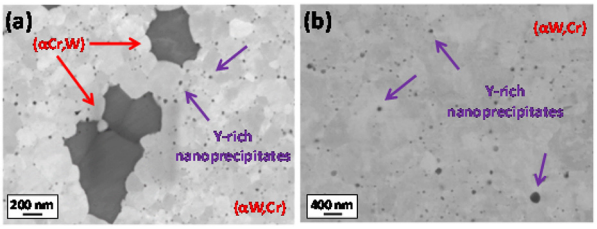

Fig. 1. FEG-SEM images of W-10Cr-0.5Y alloy (a) after HIP and (b) after HIP + TT at 1550 °C.

3. Results and discussion

The relative density and the O, C and N contents of the W-10Cr-0.5Y alloy after HIP and after TT (Table 1) are comparable to those obtained in previous works for the W-12Cr-0.5Y alloy [7].

3.1. Microstructure

After HIP, a very fine and homogeneous microstructure can be appreciated (Fig. 1(a)), with two main phases identified by EDS as a W-rich phase with Cr in solution ((αW,Cr), bright grey majority phase) and a Cr-rich phase with W in solution ((αCr,W), dark grey discontinuous phase). This microstructure is consistent with the predictions of the W-Cr phase diagram at 1250 °C [12]. The average grain size of the matrix is about 100 nm, considerably finer than that of the W-15Cr binary system, since Y acts as grain growth inhibitor, as reported in [7,16]. A dispersion of Y-rich oxide nanoparticles of about 15 nm size is formed mainly at the GB as a result of the decomposition of less stable oxides during HIPing and the high oxygen affinity of Y. This cleaning effect of GB from oxygen together with the grain refinement are supposed to be beneficial for improving the strength and toughness of the alloy at high temperature [8,16–18].

The microstructure after TT at 1550 °C is shown in Fig. 1(b) and consists of a single (αW,Cr) phase, as expected from the W-Cr phase diagram. Residual particles of (αCr,W) phase can be also found. As a consequence of the TT grain growth up to approximately 230 nm is observed in the matrix, as well as a thickening of the Y-rich oxide nanoparticles, up to about 50 nm. Further work is required to identify by TEM the composition of these nanoparticles.

3.2. Microhardness and thermal conductivity

The Vickers microhardness of W-10Cr-0.5Y alloy after HIP and after TT at 1550 °C is listed in Table 1. As reference, the microhardness of pure polycrystalline W at the corresponding average grain size is included, taking into account its Hall-Petch relationship [19]. The hardness of the as-HIPed alloy and the alloy after TT are slightly lower than that of pure W at the same average grain size, as might be expected because of the presence of a Cr-rich phase

Table 1
Relative density, impurities content, average grain size, microhardness and thermal conductivity of the W-Cr-Y alloys after HIP and after TT. For comparison, the microhardness of pure polycrystalline tungsten at the same average grain size is included.

Alloy	Relative Density (%)	Impurities (ppm)			Average grain size (nm)	Microhardness		Thermal conductivity at 600 °C [W/(mK)]
		O	N	C		Alloys ($HV_{0.5}$)	Pure W (HV) [19]	
W-12Cr-0.5Y [7]	99	1300 ± 200	90 ± 10	170 ± 10	87 ± 2	1228 ± 5	1422	55
W-10Cr-0.5Y	100	1150 ± 32	110 ± 9	140 ± 9	110 ± 4	1220 ± 8	1304	56
W-10Cr-0.5Y After TT	99	1130 ± 78	110 ± 12	160 ± 15	230 ± 11	980 ± 6	1009	–

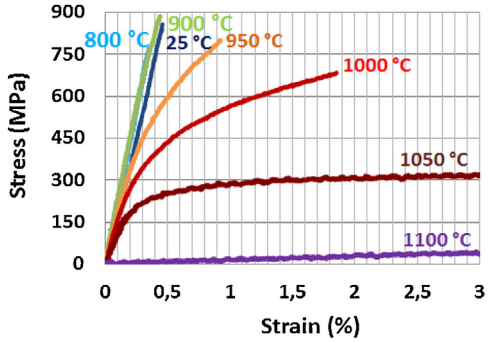

Fig. 2. Flexural strength vs strain of W-10Cr-0.5Y alloy as HIPed from 25 °C up to 1100 °C.

Table 2
Fracture toughness of W-10Cr-0.5Y alloy as HIPed.

T (°C)	25	800	900	1000	1100
F. Tough. (MPa $m^{0.5}$)	5.2	6.0	6.1	7.2	8.5
Std. Error (MPa $m^{0.5}$)	0.1	0.6	0.9	2.0	0.3

with lower hardness than W after HIP. These values are also comparable with previous results [7,20] and show the influence of grain size on hardening.

The thermal conductivity of W-10Cr-0.5Y alloy at the operation temperature (~600 °C) is about 56 W/(mK). It is lower than that of pure W due to the fact of alloying. Nevertheless, alloys of the W-Cr-Y system exhibit the highest thermal conductivity of all ternary alloys evaluated previously [7,20]. For application at the blanket FW with power densities <2 MW/m^2 [21] the resulting temperature increase for a thickness of 2–3 mm will not be a concern.

3.3. Mechanical properties

Non-standard 3PBT were performed on as-HIPed W-10Cr-0.5Y alloy from 25 °C to 1100 °C to explore its mechanical response. As can be observed in Fig. 2 the specimens showed brittle behavior up to 900 °C while some plastic deformation took place at 950 °C, therefore the ductile-to-brittle transition temperature (DBTT) lies between 900 °C and 950 °C. Although the W-Cr-Ti system presented a similar DBTT [20,22], a decrease was expected taking into account the grain size reduction [23], but there is no variation though. On the other hand, a considerable increase in flexural strength and fracture toughness at high temperature (Table 2) was observed with respect to previous works [20,22], probably because of grain refinement and improvement in the MA process. The results of 3PBT showed that the behavior of the alloy was linear elastic until fracture up to 1050 °C, temperature from which the samples exhibited plastic deformation without breaking. The primary effect of nano-dispersed Y-rich oxides in W is an increase in strength, elastic modulus and fracture toughness by inhibiting the degradation at higher temperatures as reported in [18,24].

3.4. Oxidation tests

Isothermal oxidation tests at 800 °C and 1000 °C for 60 h as well as tests under accident-like conditions up to 1000 °C were performed with the as-HIPed and HIP + TTed W-10Cr-0.5Y alloy. The mass gain during isothermal oxidation at both temperatures follows a linear kinetics with an initial parabolic phase. The oxidation rates obtained for this alloy are the lowest of all bulk systems studied so far, even lower than those for W-12Cr-0.5Y [6,7] as can be observed in Table 3.

Table 3
Linear oxidation rates, k_l, of W-10Cr-0.5Y alloy and comparison with alloys of previous works [6,7].

Alloy	k_l [mg/(cm^2 s)]	
	800 °C	1000 °C
W-15Cr	$2.9 \cdot 10^{-4}$	Delamination
W-10Cr-2Ti	$4.7 \cdot 10^{-6}$	Delamination
W-12Cr-0.5Y	$3.1 \cdot 10^{-6}$	–
W-10Cr-0.5Y	$3.9 \cdot 10^{-7}$	$7.5 \cdot 10^{-6}$

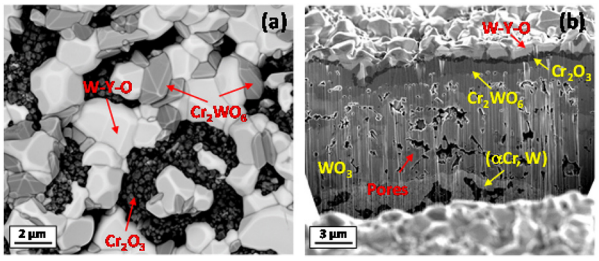

Fig. 3. FIB images of (a) surface and (b) cross section of W-10Cr-0.5Y alloy after oxidation tests at 1000 °C for 60 h.

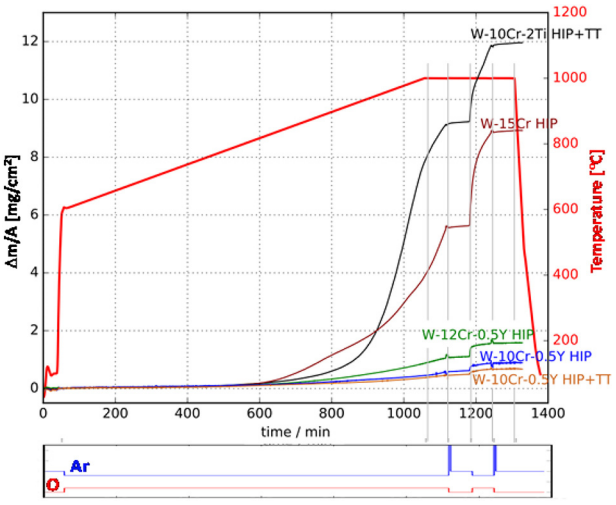

Fig. 4. Mass increase per unit area during accident-like conditions test of W-10Cr-0.5Y alloy as-HIPed and after TT compared to previous works [6,7].

The surface of the W-10Cr-0.5Y isothermally oxidized at 1000 °C and the cross section of the formed scales were analyzed by FEG-SEM, FIB and EDS (Fig. 3). At the surface, particles of Cr_2WO_6 of ~1 µm and W-Y mixed oxides of about 2 µm can be observed partly covering the thin Cr_2O_3 layer consisting of nanoparticles (light grey, white and black particles, respectively, in Fig. 3(a)). In the cross sections of the oxidized surfaces (Fig. 3(b)) three layers can be distinguished: a thin Cr_2O_3 scale partly covered with W-Y mixed oxide particles at the very surface and a thin Cr_2WO_6 layer just below, followed by a thicker WO_3 layer. It seems that the W-Y-O particles reinforce the protecting effect of the Cr_2O_3 scale leading to oxidation layers of about 14 µm thick, which is consistent with the low mass gain observed. Partial oxidation of the Cr-rich phase located near the scales was also observed. After 60 h oxidation at 800 °C the particles on the oxidized surface are smaller and the scales are thinner with an overall thickness of ~500 nm.

In contrast to the isothermal oxidation, mass increase of W-10Cr-0.5Y alloy at the second isothermal segments during the accident-like test follows a parabolic law and this alloy exhibits the best behavior against oxidation of all tested systems including W-12Cr-0.5Y alloy [6,7] as can be observed in Fig. 4. Samples subjected

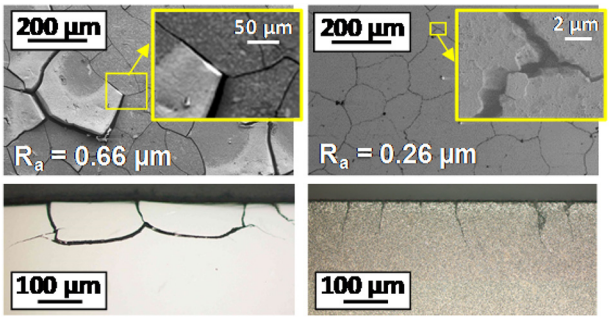

Fig. 5. Surface and cross section of W-10Cr0.5Y alloy after loading at JUDITH-1 with 1000 ELM-like pulses of 0.38 GW/m^2 for 1 ms (left) as-HIPed and (right) after TT at 1550 °C.

to TT were also studied showing a slight decrease in mass gain with respect to the as-HIPed material. Another important observation is the fact that in the isothermal segments without oxygen there is no mass loss, indicating that there is no evaporation of tungsten oxide, previously formed during the oxidation segment. The surface and oxidation scales after accident-like condition test are similar to those of Fig. 3 but the thickness and particle sizes are smaller since the overall exposition time at 1000 °C under oxidizing atmosphere is 2 h instead of 60 h in isothermal tests.

3.5. Thermo-shock tests

W-10Cr-0.5Y alloy as-HIPed and after TT was exposed to ELM-like loads. After 1000 heat pulses of 0.19 GW/m^2 for 1 ms at 400 °C no damage was detected at the surface of the samples. After 1000 pulses of 0.38 GW/m^2 the surface of the as-HIPed material was chipped whereas the sample after TT exhibited just a crack network with no chipping, as can be observed in Fig. 5. Surface roughness was reduced respect to a pure W grade reference material (IGP W) [25] under the same conditions from 0.52 µm to 0.26 µm in the HIP + TTed material. The cracks in the material after TT are clearly narrower compared to the as-HIPed material, also after disruption-like load. In this later case, only the as-HIPed sample exhibited catastrophic failure while partial melting was observed in both samples, which was also the case in the results obtained with W-10Cr-2Ti alloy in a preliminary work [20].

The alloy presents an improved performance to thermal shock loading which is likely due to the reinforcement attained in both strength and toughness at high temperatures. The very fine microstructure and the presence of Y-rich oxide nanoparticles together with the slightly higher thermal conductivity might be responsible for this improvement. The TT clearly contributes to improve the thermo-shock resistance since only a single phase is present in the material, which leads to stress relief.

4. Conclusions

A fully dense self-passivating alloy of composition W-10Cr-0.5Y (in wt.%) was produced by MA and HIP showing a very homogeneous and nanocrystalline microstructure with average grain size ~100 nm. A Y-rich oxide nanoparticles dispersion located mainly at GB inhibits grain growth and contributes to increase the strength and toughness at high temperature, which improves the material behavior under thermo-shocks loading compared to pure W reference material. The alloy exhibits the lowest oxidation rates of all developed systems, probably owing to the W-Y oxide particles formed at the surface which improve the self-passivating effect of the Cr_2O_3 scale. A final TT at 1550 °C improves the behavior of the alloy under oxidation and especially under thermal shock conditions. In view of all results, W-Cr-Y system is a promising first-wall blanket armor material.

Acknowledgments

This work has been carried out within the framework of the EUROfusion Consortium and has received funding from the Euratom research and training programme 2014–2018 under grant agreement No 633053 and by the Basque Government (ELKARTEK FRONTIERS KK-2015/00101). The views and opinions expressed herein do not necessarily reflect those of the European Commission.

References

[1] D. Maisonnier, et al., A Conceptual Study of Commercial Fusion Power Plants, Final Report, 2005.
[2] R. Neu, J. Riesch, J.W. Coenen, et al., Advanced tungsten materials for plasma-facing components of DEMO and fusion power plants, Fusion Eng. Des. (2016) 1–7.
[3] N.P. Taylor, R. Pampin, B. Birmingham, Activation properties of tungsten as a first wall protection in fusion power plants, Fusion Eng. Des. 81 (2006) 1333–1338.
[4] P. López-Ruiz, F. Koch, N. Ordás, et al., Manufacturing of self-passivating W-Cr-Si alloys by mechanical alloying and HIP, Fusion Eng. Des. 86 (2011) 1719–1723.
[5] F. Koch, J. Brinkmann, S. Lindig, et al., Oxidation behaviour of silicon-free tungsten alloys for use as the first wall material, Phys. Scr. T145 (2011) 14019.
[6] C. García-Rosales, P. López-Ruiz, S. Alvarez-Martín, et al., Oxidation behaviour of bulk W-Cr-Ti alloys prepared by mechanical alloying and HIPing, Fusion Eng. Des. 89 (2014) 1611–1616.
[7] A. Calvo, C. García-rosales, F. Koch, et al., Manufacturing and testing of self-passivating tungsten alloys of different composition, Nuclear Mater. Energy (2016) 1–8.
[8] M. Zhao, Z. Zhou, Q. Ding, et al., Effect of rare earth elements on the consolidation behavior and microstructure of tungsten alloys, Int. J. Refract. Met. Hard Mater. 48 (2015) 19–23.
[9] M. Battabyal, L. Veleva, N. Baluc, Investigation of microstructure and mechanical properties of W-Y and W-Y2O3 materials fabricated by powder metallurgy method, Int. J. Refract. Met. Hard Mater. 50 (2015) 210–216.
[10] T. Wegener, F. Klein, A. Litnovsky, et al., Development of yttrium-containing self-passivating tungsten alloys for future fusion power plants, Nucl. Mater. Energy 9 (2016) 394–398.
[11] S. Telu, R. Mitra, S.K. Pabi, Effect of Y2O3 addition on oxidation behavior of W-Cr alloys, Metall Mater. Trans. A 46 (2015) 5909–5919.
[12] W-Cr Phase Diagram, Bull Alloy Phase Diagrams, 1984, pp. 5.
[13] R. Duwe, W. Kuehnlein, H. Muenstermann, The new electron beam facility for materials testing in hot cells-design and preliminary experience, Fusion Technol. 1995 (1994) 355–358.
[14] T. Palacios, J.Y. Pastor, Influence of the notch root radius on the fracture toughness of brittle metals: nanostructure tungsten alloy, a case study, Int. J. Refract. Metals Hard Mater. 52 (2015) 44–49 (RMHM).
[15] G.V. Guinea, J.Y. Pastor, J. Planas, et al., Stress intensity factor, compliance and CMOD for a general three-point-bend beam, Int. J. Fract. 5 (1998) 103–116.
[16] M. Zhao, Z. Zhou, Q. Ding, et al., The investigation of Y doping content effect on the microstructure and microhardness of tungsten materials, Mater. Sci. Eng. A 618 (2014) 572–577.
[17] B. Gludovatz, S. Wurster, T. Weingärtner, et al., Influence of impurities on the fracture behaviour of tungsten, Philos. Mag. 91 (2011) 3006–3020.
[18] T. Palacios, A. Jiménez, A. Muñóz, et al., Mechanical characterisation of tungsten –1 wt.% yttrium oxide as a function of temperature and atmosphere, J. Nucl. Mater. 454 (2014) 455–461.
[19] E. Lassner, W.D. Schubert, Tungsten: Properties, Chemistry, Technology of the Element, Alloys and Chemical Compounds, Plenum Publishers, New York, University of Technology, Vienna, Austria, 1999.
[20] A. Calvo, N. Ordás, I. Iturriza, et al., Manufacturing of self-passivating tungsten based alloys by different powder metallurgical routes, Phys. Scr. T167 (2016) 14041.
[21] F. Arbeiter, C. Bachmann, Y. Chen, et al., Thermal-hydraulics of helium cooled First Wall channels and scoping investigations on performance improvement by application of ribs and mixing devices, Fusion Eng. Des. 111 (2015) 1123–1129.
[22] P. López-Ruiz, N. Ordás, I. Iturriza, et al., Powder metallurgical processing of self-passivating tungsten alloys for fusion first wall application, J. Nucl. Mater. 442 (2013) S219–S224.
[23] J. Reiser, J. Hoffmann, U. Jäntsch, et al., Ductilisation of tungsten (W): on the shift of the brittle-to-ductile transition (BDT) to lower temperatures through cold rolling, Int. J. Refract. Met. Hard Mater. 54 (2016) 351–369.
[24] D.T. Blagoeva, J. Opschoor, J.G. Van Der Laan, et al., Development of tungsten and tungsten alloys for DEMO divertor applications via MIM technology, J. Nucl. Mater. 442 (2013) S198–S203.
[25] M. Wirtz, J. Linke, T. Loewenhoff, et al., Thermal shock tests to qualify different tungsten grades as plasma facing material, Phys. Scr. T167 (2016) 14015.